TU Delft

Delft University of Technology

Peak Water Levels Rise Less Than Mean Sea Level in Tidal Channels Subject to Depth Convergence by Deepening

Leuven, Jasper R.F.W.; Niesten, Iris; Huismans, Ymkje; Cox, Jana R.; Hulsen, Lamber; van der Kaaij, Theo; Hoitink, A. J.F. (Ton)

DOI
10.1029/2022JC019578

Publication date
2023

Document Version
Final published version

Published in
Journal of Geophysical Research: Oceans

Citation (APA)
Leuven, J. R. F. W., Niesten, I., Huismans, Y., Cox, J. R., Hulsen, L., van der Kaaij, T., & Hoitink, A. J. F. (2023). Peak Water Levels Rise Less Than Mean Sea Level in Tidal Channels Subject to Depth Convergence by Deepening. *Journal of Geophysical Research: Oceans*, *128*(4), Article e2022JC019578. https://doi.org/10.1029/2022JC019578

Important note
To cite this publication, please use the final published version (if applicable).
Please check the document version above.

Copyright
Other than for strictly personal use, it is not permitted to download, forward or distribute the text or part of it, without the consent of the author(s) and/or copyright holder(s), unless the work is under an open content license such as Creative Commons.

Takedown policy
Please contact us and provide details if you believe this document breaches copyrights.
We will remove access to the work immediately and investigate your claim.

This work is downloaded from Delft University of Technology.
For technical reasons the number of authors shown on this cover page is limited to a maximum of 10.

Check for updates

JGR Oceans

RESEARCH ARTICLE
10.1029/2022JC019578

Peak Water Levels Rise Less Than Mean Sea Level in Tidal Channels Subject to Depth Convergence by Deepening

Jasper R. F. W. Leuven[1,2], Iris Niesten[1], Ymkje Huismans[3,4], Jana R. Cox[5], Lamber Hulsen[6], Theo van der Kaaij[3], and A. J. F. (Ton) Hoitink[1]

[1]Department of Environmental Sciences, Hydrology and Quantitative Water Management Group, Wageningen University, Wageningen, The Netherlands, [2]Royal HaskoningDHV, Resilience & Maritime (Water), Nijmegen, The Netherlands, [3]Deltares (Unit Marine and Coastal Systems), Delft, The Netherlands, [4]Faculty of Civil Engineering and Geosciences, Delft University of Technology, Delft, The Netherlands, [5]Faculty of Geosciences, Utrecht University, Utrecht, The Netherlands, [6]Port of Rotterdam, Rotterdam, The Netherlands

Abstract Effects of sea-level rise (SLR) on future peak water levels in tidal deltas and estuaries are largely unknown, despite these areas being densely populated and at high risk of flooding. While the rates of SLR accelerate, many channels simultaneously experience channel deepening for navigation. With globally decreasing sediment supplies, most channels are at risk of becoming deeper when the rate of SLR accelerates and sedimentation cannot keep pace with SLR. These factors potentially favor amplification of the tides and thereby increase flood risk, but the extent to which they will do so is unknown. Here, we introduce and use a validated model for an artificially deepened multi-branch delta to get a mechanistic understanding of non-linear SLR-effects on peak water levels. Results show that, when the current deepened bed level will be maintained, peak water levels do not rise on par with mean sea-level. Thus flood risk increases less than what can be expected from the predictions of the mean sea-level increase. The reason is that SLR causes a proportional reduction in convergence of channel area. This mechanism reduces tidal amplification. Nevertheless, SLR effects extend far beyond the range of present-day seasonal variations, with future low water levels being equal to present-day high water levels, while the tidal range slightly reduces. This will have consequences not only for flood risk, but also for freshwater availability, navigation and ecology.

Plain Language Summary Many urban deltas are becoming deeper, often due to dredging for navigation purposes. A larger channel depth decreases friction, leading to amplification of the tide (higher peak water levels). At the same time, climate projections predict accelerated Sea-Level Rise (SLR). SLR also increases the channel depth, thereby amplifying the tide. However, it is unknown to which extent SLR and channel deepening increase peak water levels. Here, we use a validated model of the Rhine-Meuse Delta to study the effect of SLR and channel deepening on peak water levels. Results confirm that local dredging of the channel increases peak water levels. The larger depth at the mouth increases the convergence of cross-sectional channel area in landward direction. This convergence is known to increase the tidal amplitude in landward direction, also known as tidal amplification. In contrast, peak water levels do not rise on par with SLR when the current deepened bed level is maintained. This is because the landward reduction in channel area diminishes with SLR. Nevertheless, future low water levels are predicted to be equal to present-day high water levels, while the tidal range slightly reduces. This will have consequences for flood risk, freshwater availability, navigation and ecology.

Key Points:

- Channel deepening can immediately amplify tides, which over the course of time may partially be counteracted by sea-level rise (SLR)
- In depth-convergent artificially deepened channels, SLR reduces tidal amplification
- The reduction in tidal amplification causes the peak water levels to rise less than mean sea level

Supporting Information:

Supporting Information may be found in the online version of this article.

Correspondence to:

J. R. F. W. Leuven, I. Niesten, and A. J. F. Hoitink,
jasper.leuven@rhdhv.com;
iris.niesten@wur.nl;
ton.hoitink@wur.nl

Citation:

Leuven, J. R. F. W., Niesten, I., Huismans, Y., Cox, J. R., Hulsen, L., van der Kaaij, T., & Hoitink, A. J. F. (2023). Peak water levels rise less than mean sea level in tidal channels subject to depth convergence by deepening. *Journal of Geophysical Research: Oceans*, *128*, e2022JC019578. https://doi.org/10.1029/2022JC019578

Received 26 JAN 2023
Accepted 14 MAR 2023
Corrected 12 APR 2023

This article was corrected on 12 APR 2023. See the end of the full text for details.

Author Contributions:

Conceptualization: Jasper R. F. W. Leuven, Iris Niesten, Ymkje Huismans, A. J. F. (Ton) Hoitink

© 2023 The Authors.
This is an open access article under the terms of the Creative Commons Attribution-NonCommercial License, which permits use, distribution and reproduction in any medium, provided the original work is properly cited and is not used for commercial purposes.

1. Introduction

Deltas are typically densely populated areas (Ashworth et al., 2015; Edmonds et al., 2020), in which the distributaries are of special importance because they provide access to inland harbors (de Vriend et al., 2011; Hoitink et al., 2020). Many deltas are under pressure from changing boundary conditions and human influence, including sea-level rise (SLR) (Giosan et al., 2014; Khojasteh et al., 2021; Leuven et al., 2019; Oppenheimer & Hinkel, 2019), land subsidence (Minderhoud et al., 2018; Syvitski et al., 2009) and dredging for reasons of navigation and sand mining (Bendixen et al., 2019; Cox, Dunn, et al., 2021; Hackney et al., 2020; van Dijk et al., 2021; Wu et al., 2016). The complex interplay between tides, storm surges and the river discharge causes that the effects of dredging and relative SLR on peak water levels can change across a delta plain (Bao et al., 2022). Although dredging and channel deepening tend to be local measures, typically focused on one navigation channel or one

Data curation: Jasper R. F. W. Leuven, Iris Niesten, Jana R. Cox
Formal analysis: Jasper R. F. W. Leuven, Iris Niesten
Funding acquisition: A. J. F. (Ton) Hoitink
Investigation: Jasper R. F. W. Leuven, Iris Niesten
Methodology: Iris Niesten, Lamber Hulsen, Theo van der Kaaij
Software: Lamber Hulsen, Theo van der Kaaij
Validation: Jasper R. F. W. Leuven, Iris Niesten, Lamber Hulsen
Visualization: Jasper R. F. W. Leuven
Writing – original draft: Jasper R. F. W. Leuven, Iris Niesten, Jana R. Cox
Writing – review & editing: Ymkje Huismans, A. J. F. (Ton) Hoitink

section of a channel, they may have an overarching effect on the hydrodynamics and associated peak water levels of the entire estuary (Talke & Jay, 2020).

Observations from individual estuaries have indicated that dredging can decrease channel roughness, increase tidal amplitudes, enhance depth convergence, decrease flood wave attenuation and reduce tidal dampening and storm surge dampening (Familkhalili et al., 2020; Muñoz et al., 2022; Talke et al., 2021; Talke & Jay, 2020). Capturing this behavior in modeling has proved challenging (Cai et al., 2012), particularly when estuaries are heavily anthropogenically influenced, and move away from classic, width converging estuary morphology, such as in the Rhine-Meuse Delta (RMD) in The Netherlands (Cox, Lingbeek, et al., 2022) and the Pearl Delta in China (Bao et al., 2022). With channel deepening, the tidal range generally increases and storm surge waves also amplify, while high river discharge events generally exert a smaller control on peak water levels in the delta channels (Talke et al., 2021). Understanding and disentangling the effects of dredging from the effects of climate change is both important and challenging (Bao et al., 2022; Cox, Lingbeek, et al., 2022).

Many natural estuaries and deltas are not in a state of (quasi-)morphological equilibrium. Neither do the channels satisfy generic relations between tidal prism and cross-section area, nor does the tidal energy dissipation balance channel area convergence such that the tidal amplitude remains roughly constant, as in an ideal estuary. Nevertheless, many delta channels are characterized by some level of width or depth convergence (Leuven et al., 2018). Navigation channels toward multiple harbor basins in deltas are generally depth convergent: depth decreases when navigating landward, albeit not necessarily monotonously. Typically, the largest ships moor in the deepest, seaward harbors, and the smaller ships, with smaller draft, can navigate toward the shallower harbor basins located further inland (Cox, Dunn, et al., 2021). In this study, we specifically focus on peak water levels in such tidal channels subject to depth convergence by deepening.

Future peak water levels are an important consideration for flood safety (Buchanan et al., 2017; O'Neill et al., 2020; Purvis et al., 2008), but the effect of climate change on peak water levels within delta branches remains under-explored. Factors affecting peak water levels include the future increased mean water level (roughly 1 m in the coming century for the RCP8.5 scenario) (Haasnoot et al., 2018; Masson-Delmotte et al., 2021; Portner et al., 2022; van Dorland, 2021), more extreme fluvial discharge (Ganguli & Merz, 2019), increased tidal prism (Leuven et al., 2019; Pickering et al., 2017) and increased flood dominance (Friedrichs et al., 1990). Earlier data analysis suggests that the relation between high water levels and SLR might be less than one-on-one, while mean sea-level increases linearly with SLR (Vellinga et al., 2014; Yang et al., 2015). Here, we systematically model those effects to test the relation between SLR and peak water levels in an area where tides are the primary forcing factor. In other parts of the delta, flood risk can be controlled by other forcings, such as river discharge (Orton et al., 2020).

The RMD (Figure 1) is an example of a deepened multi-branch delta that has undergone many human interventions (Cox, Huismans, et al., 2021; Huismans et al., 2021; Vellinga et al., 2014). Hydrodynamic data have been collected since the 1930s (Vellinga et al., 2014) (Figure 1), which enables model validation and calibration. While the current hydrodynamic conditions of this multi-branch delta have been reported by Cox, Dunn, et al. (2021) and Cox, Huismans et al. (2021), the future conditions with SLR and the impact of SLR on the water levels have not yet been explored in scientific literature. The location of the branches has been fixed during the entire time period from the 1930s. So, while the depth profiles of the channels have been subject to change, the width of the channels have remained virtually unchanged.

We use realistic scenarios based on historic conditions to understand the natural variability of hydrodynamic conditions under variable discharge and storm conditions causing wind set-up. We subsequently assess how tidal peak water levels will evolve as a result of a larger channel depth due to future SLR and human intervention, such as active channel deepening.

Many other deltaic systems around the world are already at an extreme degree of urban development, while several other systems have not yet reached this stage (Cox, Dunn, et al., 2021). Because the RMD represents a tidal delta with artificially deepened channels similar to those toward many other ports in the world, this study has wider implications regarding the relative impact of anthropogenic interventions and SLR on future functioning, and can inform to improve management strategies (Temmerman et al., 2013; Temmerman & Kirwan, 2015). This is particularly pertinent as deltas will experience climate related challenges including SLR, storms and more frequent high discharge events (Oppenheimer & Hinkel, 2019).

21699291, 2023, 4, Downloaded from https://agupubs.onlinelibrary.wiley.com/doi/10.1029/2022JC019578 by Tu Delft, Wiley Online Library on [09/05/2023]. See the Terms and Conditions (https://onlinelibrary.wiley.com/terms-and-conditions) on Wiley Online Library for rules of use; OA articles are governed by the applicable Creative Commons License

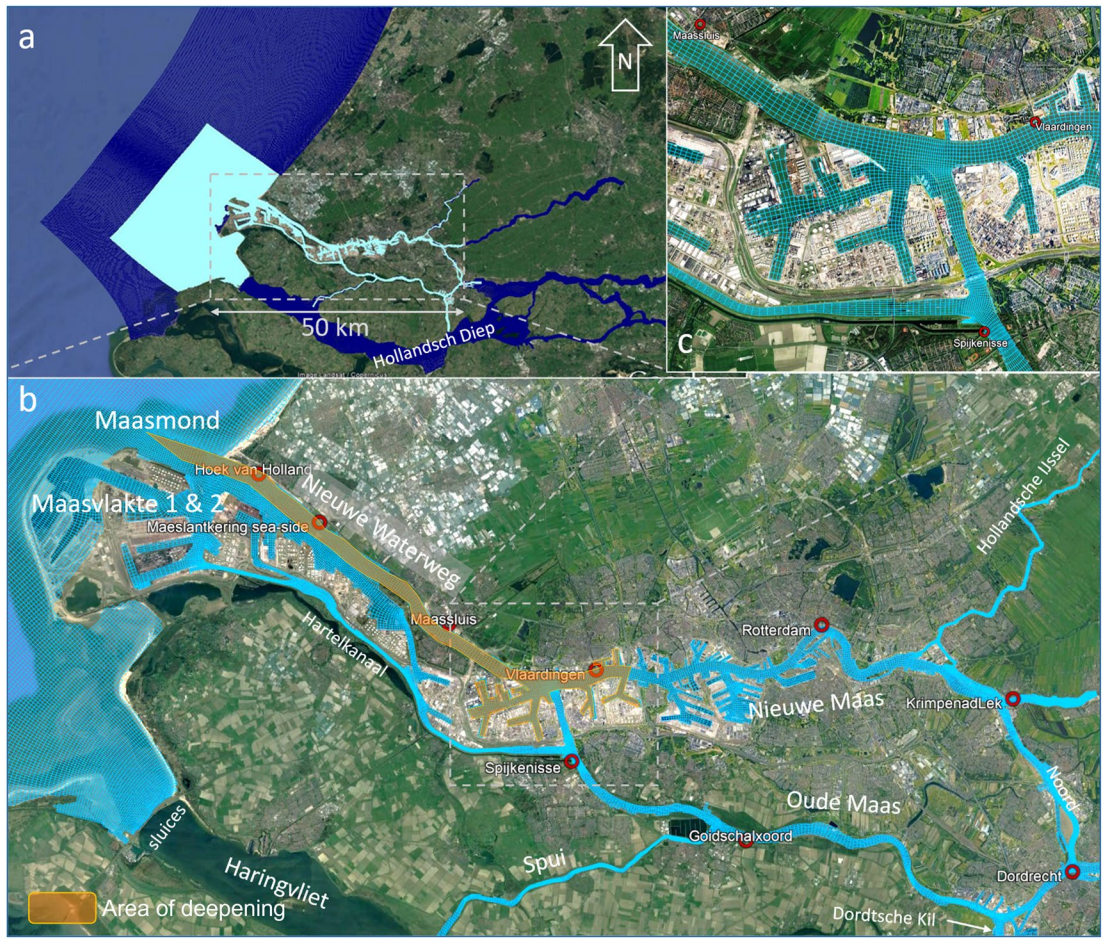

Figure 1. Aerial photographs of the Rhine-Meuse Delta, along with the model domain and names of the branches. (a) Model domain. The dark blue area indicates the larger 2D-model from which the smaller 3D-model (light blue) derives its boundary conditions. Both domains have the same grid size. (b) Model grid of the smaller 3D-model with red circles indicating the locations of measurement stations that were used for model validation. (c) Inset of the model grid at the bifurcation from the Nieuwe Waterweg (West) to the Nieuwe Maas (East) and the Oude Maas (South).

We investigate how hydrodynamic conditions in the RMD vary as a result of natural conditions under SLR, based on scenario's of human interference with a finite volume, 3D-hydrodynamic model. We first model six sets of conditions from the recent past, ranging from high fluvial discharge (≈4,000 m^3/s) to low fluvial discharge (≈1,250 m^3/s) based on statistics (Lenderink et al., 2007), and with and without wind-induced water level set-up at the mouth (≈1 m of wind set-up) (see Table 1 and the methods section). From this, we derive typical hydrodynamic conditions and the natural variation thereof. Because we considered historic conditions with natural variations in the tidal motion and wind forcing, the highest discharges do not necessarily lead to the highest water levels at the mouth, as water levels at the mouth are primarily governed by the sea levels.

Subsequently, we implement seven scenarios with 1 m SLR and three scenarios of human interference, to study their effect on peak water levels under varying conditions of discharge and wind setup. From this, we infer the impact of changing depth due to SLR or active channel deepening on system behavior and peak water levels, and discuss implications for other deltas worldwide.

2. Geographical Setting of the Rhine-Meuse Delta Mouth

The RMD hosts a deepened channel system where human measures are motivated by flood safety and fresh water supply considerations, and navigation to the Port of Rotterdam network (Figure 1). Due to extensive embankments, land reclamation, narrowing and deepening and construction of new waterways between 1500 and present, the system no longer resembles a classic estuary or delta channel network (Cox, Leuven, et al., 2022; Huismans

21699291, 2023, 4, Downloaded from https://agupubs.onlinelibrary.wiley.com/doi/10.1029/2022JC019578 by Tu Delft, Wiley Online Library on [09/05/2023]. See the Terms and Conditions (https://onlinelibrary.wiley.com/terms-and-conditions) on Wiley Online Library for rules of use; OA articles are governed by the applicable Creative Commons License

21699291, 2023, 4, Downloaded from https://agupubs.onlinelibrary.wiley.com/doi/10.1029/2022JC019578 by Tu Delft, Wiley Online Library on [09/05/2023]. See the Terms and Conditions (https://onlinelibrary.wiley.com/terms-and-conditions) on Wiley Online Library for rules of use; OA articles are governed by the applicable Creative Commons License

Table 1
Overview of Model Runs Used in This Study

(a) Model runs with historical boundary forcing

		Bathymetry			
Q_r (m^3/s)	Wind set-up (m)	Corresponding	2019	2019 + deepening	With 1 m SLR
High (≈4,500)	No (<0.3)	V1	R1		SLR1
High (≈4,500)	Yes (≈1)	V2	R2		SLR2
Med (≈2,000)	No (<0.3)	V3	R3		SLR3
Med (≈2,000)	Yes (≈1)	V4	R4	D4	SLR4
Low (≈1,250)	No (<0.3)	V5	R5		SLR5
Low (≈1,250)	Yes (≈1)	V6	R6		SLR6

(b) Model runs with extreme boundary forcing ($TR \approx 1/100$).

		Bathymetry			With
Q_r	Wind	2019	1 m shallowing	1 m deepening	1 m SLR
Med (≈2,000)	1/100	E	E-SLR-S	E-SLR-D	E-SLR

Note. The top part of the table (a) displays the runs with boundary conditions based on historical data. Runs with name **V**x refer to validation runs, **R**x refers to reference runs, **D**x to runs where the navigation channel has been deepened with 1 m, and **SLR**x refers to model runs with 1 m sea-level rise compared to the original forcing. The bottom part of the table (b) shows model runs with fictional boundary conditions. Boundary conditions are composed of river discharge and wind set-up, the combination of which has a return time (RT) of 1/100 years. Simulation name **E**x refers to extreme boundary conditions. The boundary forcing in part A corresponds to the validation periods and is based on historical events. For the exact periods we refer to the supplementary material. For the **V**x-runs bed levels were used that correspond to the validation period. Shortly after that (in 2019) the bed has been deepened, which is why the reference runs were used for further analysis in this paper.

et al., 2021). Channel depths are controlled by dredging, particularly in the Nieuwe Maas and Nieuwe Waterweg branches. Several deepening events have taken place since the 1950s, driven by increasing ship size (Cox, Dunn, et al., 2021). As many estuaries and deltas are undergoing similar changes globally (engineering works, dredging for port access, embankments and dikes for flood protection), it represents a new state for estuaries: an archetypical urban estuary.

The mouth of the RMD is composed of a northern outlet (through the Nieuwe Maas and Nieuwe Waterweg channels, respectively) and a southern outlet (through the Hollands Diep, Haringvliet waterways), which is closed by a dam. The northern and southern branches are connected by a set of cross-cut tidal channels with several bifurcations and confluences (Figure 1). Three upstream rivers feed the delta area: the Waal, Maas, and Lek which on average convey 70%, 14%, and 16% of the discharge, respectively. The main route of water is first via the south (Waal/Nieuwe Merwede to Hollands Diep), after which most water flows back north via the cross-cut channels to the Nieuwe Waterweg/Maasmond. On the seaward boundary, a net discharge of about 1,400 m^3/s debouches to sea via the northern outlet (Cox, Huismans, et al., 2021). A further net discharge of about 220 m^3/s is typically debouched via the Haringvliet sluices at the southern outlet under average river discharge conditions (Figure 1).

The southern outlet (Haringvliet) was closed to the tides in 1970 by a complex of sluices known as the Haringvliet sluices (Figure 1b). During periods of low river discharge, the sluices are closed, which ensures that ample fresh water flows through the Nieuwe Waterweg to counteract salt intrusion. During high and average river discharge conditions, the sluices are fully open at low-tide. Then, the river discharge that previously would be redirected north, via the cross-cut channels to the Nieuwe Waterweg, leaves the system via the sluices. Until 2019, the sluices were always fully closed during high tide. Since 2019, they are partially opened for fish migration. This process, known as the "steering" of the Haringvliet sluices, strongly influences the hydrodynamics of the region, in particular the distribution of discharge over distributaries and the tidal propagation and tidal prism in the branches.

In case of storm surge events, the mean discharge and tidal propagation in the northern and cross-cut channels can reverse (Cox, Huismans, et al., 2021). During extreme storm surge, leading to water levels exceeding 3 m above mean sea level in Rotterdam, the storm surge barrier in the Nieuwe Waterweg (the Maeslantkering) closes, to prevent the hinterland from flooding. As in many other deltas worldwide, peak flows in rivers are projected

21699291, 2023, 4, Downloaded from https://agupubs.onlinelibrary.wiley.com/doi/10.1029/2022JC019578 by Tu Delft, Wiley Online Library on [09/05/2023]. See the Terms and Conditions (https://onlinelibrary.wiley.com/terms-and-conditions) on Wiley Online Library for rules of use; OA articles are governed by the applicable Creative Commons License

to increase (Quante & Colijn, 2016), which will determine how the Haringvliet sluices are steered and how discharge is distributed over the branches.

The RMD region has multiple tidal bifurcations. The cross-cutting tidal channels connecting the northern outlet and the southern outlet, experience extremely high tide-driven water level gradients. This has caused severe erosion in some branches and local scour (Huismans et al., 2021). Tidal intrusion extends beyond Dordrecht during low discharge conditions. In this study, we focus on the area from the river mouth (Maasmond) up to the extent of inland tidal influence (approximately the city of Dordrecht), such that we cover two separate branches from bifurcation to confluence (Figure 1c).

3. Methods

In this section, the methodological aspects of the modeling approach are given including boundary and initial conditions, followed by a description of the used model sets, model validation and post-processing of model results.

3.1. Numerical Hydrodynamic Modeling

In the RMD, salt intrusion and the associated 3D flow dynamics in the branches may impact the tidal dynamics. A 3D model was therefore employed derived from an operational hydrodynamic forecasting model in Delft3D, solving the shallow water equations under the assumption of hydrostatic, non-compressible flow (Deltares, 2021). The operational model is developed and calibrated for predictions of water level and salinity throughout the area, selecting bed roughness by calibration. With respect to the operational model, the bathymetry and boundary and initial conditions were updated for this study. Other model settings remained unaltered, and we did not recalibrate the model. A full description of the model settings can be found in (Kranenburg, 2015a, 2015b), which also includes an elaborate validation. A short description of the model setup (Sections 3.1.1 and 3.1.2) and validation for our periods of interest (Section 3.1.4) is provided here for convenience.

In Delft3D, the 3D viscosity and diffusion terms are represented by a k-ϵ-model, for turbulence closure. The k-ϵ-model was chosen, as this is the most stable turbulence model for flow with high density gradients. The hydrodynamic model was coupled online to Delft3D-WAVE (Deltares, 2014), which adds energy dissipation as a result of wave action to the momentum equations.

3.1.1. Model Geometry

The hydrodynamic model domain covers the central and northern branches of the RMD (Figure 1) including part of the North Sea, covering an offshore domain of 18 × 20 km. The horizontal grid resolution is approximately 400 × 175 m in the offshore area, and increases to approximately 80 × 20 m in the smaller inland channels. The cell size in the Nieuwe Waterweg and Nieuwe Maas is approximately 140 × 80 m, corresponding to 6 computational cells over the channel width. In the vertical, the computational grid consists of 10σ-layers, implying that the vertical layer thickness varies with depth. The thickness of the layers increases stepwise from 6% to 12% of the water depth, with the thinnest layers near the bed.

The bed levels of the inland channels and ports are derived from regular surveys carried out by the Port of Rotterdam and the Dutch Ministry of Infrastructure and Water Management. The offshore bathymetry is based on a bathymetric survey from 1999, with the exception of the region around Maasvlakte 2, which was updated in 2013. The bathymetry of the validation runs (Table 1) is derived from the surveys in the corresponding years. The bathymetry of the reference runs and deepening scenario are based on more recent surveys carried out in 2019. All bed level-files are made available with the models in a data repository (see Data Availability Statement).

The bed roughness is defined by a Manning roughness, resulting from hydrodynamic calibration of the operational model. Manning coefficients vary between 0.015 s $m^{1/3}$ in the deep navigation channels and 0.030 s $m^{1/3}$ in the upstream riverine area. Subsequently, a water depth dependent Chézy value is calculated in the model.

We assume that boundaries along the model domain cover the maximum area that is inundated at high water levels, due to the presence of dikes and high embankments. In some cases, minor side-channels were not implemented in the model-grid due to their small size, that is, smaller than the model grid size. In addition, some isolated patches of intertidal area were not included. It is assumed that the model boundaries will not change due to SLR, for

21699291, 2023, 4, Downloaded from https://agupubs.onlinelibrary.wiley.com/doi/10.1029/2022JC019578 by Tu Delft, Wiley Online Library on [09/05/2023]. See the Terms and Conditions (https://onlinelibrary.wiley.com/terms-and-conditions) on Wiley Online Library for rules of use; OA articles are governed by the applicable Creative Commons License

Table 2
Overview of the Periods Upon Which All Boundary Conditions are Based

Model run	Simulation period	Period of interest
1	25/05/2016	21/06/2016
	04/07/2016	23/06/2016
2	15/01/2016	06/02/2016
	12/02/2016	08/02/2016
3	01/05/2016	06/05/2016
	15/05/2016	08/05/2016
4	27/09/2014	21/10/2014
	26/10/2014	22/10/2014
5	25/09/2015	10/10/2015
	20/10/2015	12/10/2015
6	26/11/2014	10/12/2014
	14/12/2014	12/12/2014
Extreme	07/11/2013	05/12/2013
	12/12/2013	06/12/2013

Note. Numbers 1 to 6 refer to the simulation numbers of model set (a); Extreme refers to model set (b) (see Table 1). The simulation time is longer than the period of interest to prevent spin-up effects.

example, that areas that currently do not flood at high tide will also not flood under SLR. In practice, there will be a few smaller patches along the model domain that may or may not flood under SLR. Together, they may contribute a maximum of 10% in surface area under SLR, which probably slightly enhance the effect of reduced amplification under SLR that was found in the main results of this paper. This is a valid assumption in urbanized systems, where intertidal areas have often been subject to land reclamation.

3.1.2. Derivation of Boundary and Initial Conditions

All boundary conditions of the hydrodynamic Delft3D model are derived from a 2D large-domain model. The large-domain model is set up in the WAQUA-software, which is the predecessor of Delft3D-FLOW (De Goede, 2020). WAQUA stands for WAter movement and water QUAlity modeling. The horizontal model grid of the WAQUA-model is equal to the Delft3D-model grid in the overlapping model domain. The WAQUA-model is forced upstream by measured discharge of the rivers Hollandse IJssel, Lek, Waal and Meuse. The upstream boundaries are located where river discharge is controlled by a weir or where no tidal influence is visible, neither in the flow velocity nor in water levels. Next to that, wind forcing is applied based on the measured wind speed and direction at Hoek van Holland.

The seaward boundary conditions of the WAQUA model consist of Riemann invariants. The boundary conditions are derived in two steps. First, an initial computation is carried out using astronomic tidal water levels at the seaward boundaries. Upstream forcing consists of measured river discharge, and a wind field is derived from the measured wind speed and direction at Hoek van Holland station. Using Kalman-filtering, the seaward boundary conditions are then corrected, so that the modeled water levels correspond to the measured water levels at 5 measuring stations located within the North Sea. These data reference stations are: Scheveningen, Hoek van Holland, Lichteiland Goeree, Haringvliet 10 and Brouwerhavensche Gat08 (see Figure S1 in Supporting Information S1 for a map with locations). A second simulation is then carried out with the same upstream forcing, and assimilated seaward forcing. From this simulation, boundary conditions for the small 3D-model domain are retrieved, consisting of Riemann boundaries at sea and discharge time series at the upstream boundaries and at the Haringvliet sluices in the South.

The forcing of the 3D-hydrodynamic model consists of discharge boundary conditions at the landward boundaries (rivers Hollandse IJssel, Lek and Beneden Merwede and the tidal channels Dordtsche Kil and Spui), and water level time series at the North Sea boundary. The depth- and time-varying salinity at all open boundaries is derived from the WAQUA model. The wind forcing of the 3D-model is equal to the wind forcing of the large-scale WAQUA model. Initial conditions consist of water level, current velocity and direction and salinity in the full model domain, which are derived from the large domain WAQUA model. The simulations include a spin-up time of 2 weeks.

The boundary conditions of all model simulations are based on historical time-series. An overview of these periods is given in Table 2. For all periods, time series of the water levels at the 5 data assimilation stations, discharge at the river boundaries and wind speed and direction at Hoek van Holland were available with a 10-min measuring interval. For the validation and reference runs, the model boundary forcing is derived from the unaltered water level and discharge time-series. The boundary forcing of the SLR-runs is obtained by adding 1 m to the measured water levels at the data assimilation stations, and recomputing the boundary conditions with the large-domain model. The upstream river discharge remains unaltered.

Apart from the historical boundary conditions, we run an extreme scenario to study the effect of changing depth on peak water levels under extreme conditions, that is, storm conditions leading to a high water level with a return frequency of 1 per 100 years. The boundary conditions of this extreme scenario (model set B, Table 1) are based on wind and water level measurements of a historic storm event which took place in December 2013. The measured peak water level during this storm at Hoek van Holland has a return frequency of 120 high waters per 1,000 years (Kroos, 2014). In order to obtain a high water level which has a return time of 1 in 100 years, the

21699291, 2023, 4, Downloaded from https://agupubs.onlinelibrary.wiley.com/doi/10.1029/2022JC019578 by Tu Delft, Wiley Online Library on [09/05/2023]. See the Terms and Conditions (https://onlinelibrary.wiley.com/terms-and-conditions) on Wiley Online Library for rules of use; OA articles are governed by the applicable Creative Commons License

setup (equal to the measured water level minus the astronomical water level) was transformed to obtain the 1/100 peak water level:

$$h_{HvH,1/100} = h_{HvH,astro} + f(h_{HvH,measured} - h_{HvH,astro}) \quad (1)$$

where $h_{HvH,1/100}$ denotes the Hoek van Holland-water level with a return period of 1/100 years, $h_{HvH,\ astro}$ is the astronomical water level at Hoek van Holland, and $h_{HvH,\ measured}$ the measured water level at Hoek van Holland during the 2013-storm. The transformation factor f was determined from the difference between the known 1/100-water level and the measured water level, and equals 1.36. The same factor was used to transform the measured water levels at the remaining data assimilation stations. The measured wind speed was altered such that the peak velocity matches the 1/100-conditions. Subsequently, the transformed water level and wind speed are applied as forcing in a large-domain model computation, from which the boundary conditions for the Delft3D-model are derived. Both the water level with a return period of 100 years, and the corresponding wind speed are the results from a flood protection design study (Duits & Kuijper, 2017). The return period of the local water levels was determined statistically based on water level measurements dating back to 1890 (Kramer et al., 2017). Based on analysis of the historical simulations, we infer that the water level at Hoek van Holland station is tide and wind dominated, whereas discharge plays a minor role. Hence, we assume that the water level set-up at Hoek van Holland in this scenario is fully driven by wind. Therefore, the river discharge forcing remains unaltered with respect to the 2013-storm event. Also the wind direction (West) remains unaltered.

3.1.3. Description of Model Sets

The model simulations are divided in the following categories (see also Table 1):

- Validation runs: The boundary conditions of the validation and reference runs were chosen to cover a wide range of often recurring conditions. Conditions range from low river discharge (≈1,250 m^3/s) combined with zero wind setup to high river discharge (≈4,000 m^3/s) combined with high wind set-up. For each model, the bathymetry from surveys in the corresponding year was used. This means that model geometry and bathymetry varied among models in this set. These runs were used to validate model performance against measurements (see below).
- Reference runs: The reference runs differ from the validation runs in bathymetry. The bathymetry of all runs within this set is based on the more recent surveys carried out in 2019. This allows for intercomparison within this set and for comparison between the reference runs and model set with SLR. The boundary conditions of the reference runs are based on the validation periods, but are recomputed by running the large domain model with the 2019-bathymetry, for consistency and to prevent flow instabilities at the boundaries.
- SLR runs: The full set of SLR-runs contains the same 2019-bathymetry as the reference runs. The boundary conditions are altered to include 1 m SLR.
- Deepening scenario: The 2019-bathymetry is adapted to simulate a 1 m deepening of the fairway. To this aim, all harbors and channels within the Nieuwe Waterweg and part of the Nieuwe Maas are further deepened with 1 m (see Figure 1). We chose to only compute a deepening scenario with the boundary forcing of period 4, as this period contains the highest high water levels. The boundary conditions are again re-computed with the large-domain model and the adapted bathymetry.
- Extreme forcing: the bathymetry of all runs within this set were based on the 2019-bathymetry. Next to the bathymetry with 1 m deepening, a bathymetry was constructed with a 1 m shallowing, covering the same area. The boundary conditions were chosen to represent a storm event with a return period of 100 years.

To focus on the system response, the storm surge barrier in the Nieuwe Waterweg (the Maeslantkering) will never close in the simulations. Moreover, it is not yet clear what will happen with the closing frequency or barrier itself in the future.

In all cases we consider the compound effect of all conditions (Moftakhari et al., 2017), for example, the combined effect of high river discharge, wind set-up and SLR. This is also called "a flooding assessment approach that accounts for the compounding effects of fluvial flooding and coastal sea level" (Moftakhari et al., 2017).

3.1.4. Model Validation

We validated the model results with data from measurement stations within the modeling domain (Figure 1b). Measured water levels at those stations and wind conditions at the seaward boundary (Hoek van Holland) were

21699291, 2023, 4, Downloaded from https://agupubs.onlinelibrary.wiley.com/doi/10.1029/2022JC019578 by Tu Delft, Wiley Online Library on [09/05/2023]. See the Terms and Conditions (https://onlinelibrary.wiley.com/terms-and-conditions) on Wiley Online Library for rules of use; OA articles are governed by the applicable Creative Commons License

available from Rijkswaterstaat (waterinfo.rws.nl and noos.matroos.rws.nl). Validation results are shown in Supporting Information S1.

The root-mean-square-error (RMSE) in the model was between 0.05 and 0.17 m, and the bias was found to be between −0.06 and 0.12 m. RMSE and bias were typically larger for the model simulations with higher discharge. The mismatch was mostly found for low water levels at the landward side of the model domain, where the model predicts slightly lower low water levels than measured.

3.2. Post-Processing and Data Reduction

For each model, along-channel profiles were extracted along the centerlines of the channel. Along those lines, tidal range, minimum and maximum water levels were determined. For further data reduction, four typical locations were selected along the RMD. One in the seaward zone (at the Maeslantkering), one in the middle zone for each branch (at Rotterdam and at Goidschalxoord stations), and one at the landward zone (at Dordrecht), where the branches confluence again (Figure 1b). For those locations, the effects of boundary conditions and SLR effects were studied in greater detail.

4. Results

4.1. Natural Variation in Hydrodynamic Conditions

Model results show that, in general, the tides dampen slightly from the mouth (Maasmond) toward the bifurcation of the Nieuwe Maas and Oude Maas (Figure 2). For the conditions subject to this study, the tidal range is typically within 2.0–3.5 m, with high water levels at about 2.5 m NAP during storm surge and low water levels of −0.8 m NAP. Herein, NAP means Amsterdam Ordnance Datum, or "Normaal Amsterdams Peil", which is the Dutch reference level for elevation, with 0 m NAP being at approximately mean sea level.

From the bifurcation in landward direction, the hydrodynamic conditions vary significantly among the branches: tides amplify along the seaward stretch of the Nieuwe Maas channel up to the city of Rotterdam, while they dampen rapidly along the Oude Maas branch. Landward of the bifurcation, the Nieuwe Maas remains deep, and shallows in a few steps from −17 to −12 m NAP, while channel width converges. In contrast, the Oude Maas channel initially shallows to about −12 m NAP and then deepens again up to −19 m NAP. The degrees of channel width and depth convergence explain the amplification of the water levels in the northern branch, and the damping in the southern branch.

Wind set-up has a dominant effect on water levels along the branches, increasing high water levels by 0.5–1 m and thereby increasing the tidal range (Figure 2). In absence of wind set-up, a higher fluvial discharge coincides with an increase in high water levels in the most landward reach and a decrease in low water levels in the seaward reach. The most extreme scenario in this set is scenario 4. In this scenario, a long period of high wind-speed from northwestern direction resulted in a wind set-up of up to 1.2 m at Hoek van Holland, at the coastal boundary.

4.2. Effects of SLR on Peak Water Levels

For all those conditions, the effect of 1 m SLR was examined, and for Scenario 4 this was also contrasted to the effect of deepening the channels by 1 m. Lastly, we followed-up with an extreme scenario that is representative of conditions that would occur at approximately once in a 100 years after sea-level has risen by 1 m, and investigate the effects of further deepening and the mitigating potential of shallowing the channels.

Peak water levels increase in all cases and along the entire delta by less than 1 m as a result of 1 m SLR (Figure 3a). Even under mild conditions (e.g., without wind set-up), 1 m SLR results in peak water levels that are as high as the current peak water levels under the considered extreme conditions. At the same time, surprisingly, the tidal range decreases (Figure 3b), mainly caused by peak water levels increasing a bit less than the 1 m of SLR (Figure 4a), while low water levels remain mostly the same or increase slightly (Figure 4b). This results in tidal ranges that are slightly smaller than without SLR (Figure 3b). Part of the anticipated decrease in tidal range might be negated in the future by a shift of amphidromic points (i.e., tidal nodes) on the open sea, which will increase tidal amplitude at the mouth (Idier et al., 2017; Leuven et al., 2019; Pickering et al., 2017).

The effect of SLR on high and low water levels depends on three factors: (a) the location along the system due to along-channel variations in depth and width, (b) the fluvial discharge and (c) whether wind caused significant

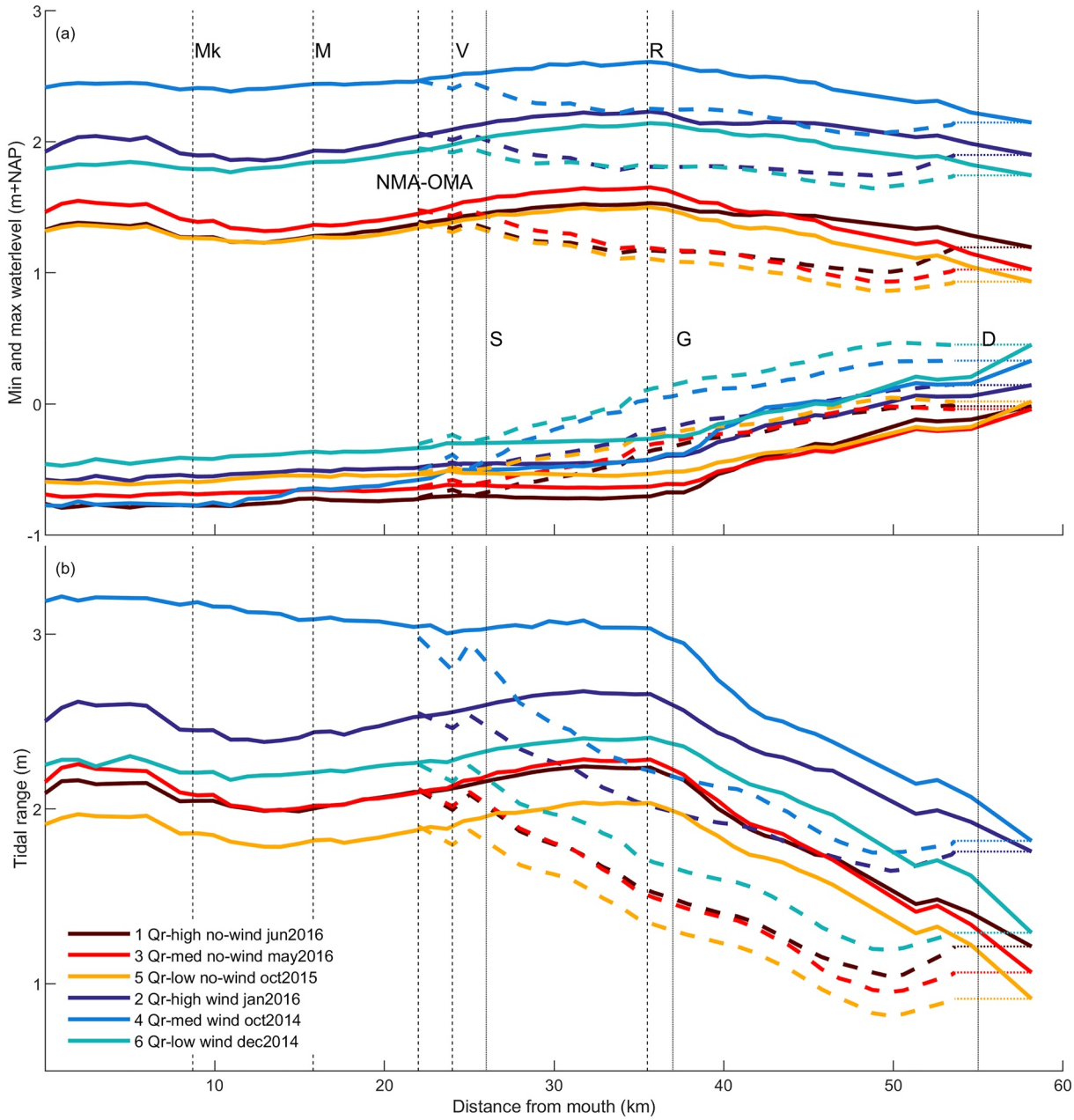

Figure 2. Along-channel variation in (a) maximum and minimum water levels and (b) tidal range. NMA-OMA indicates the confluence of the Nieuwe Maas and the Oude Maas into the Nieuwe Waterweg. The Nieuwe Maas and Nieuwe Waterweg are indicated with a solid line, the Oude Maas with a dashed line. Locations along the channels are indicated with letters and dashed vertical lines. Along the Nieuwe Waterweg: Mk = Maeslantkering, M = Maassluis. Along the Nieuwe Maas: V = Vlaardingen, R = Rotterdam. Along the Oude Maas: S = Spijkenisse, G = Goidschalkxoord, D = Dordrecht.

water level set-up (Figure 4). In the most seaward part of the delta, the effects of SLR on high water levels are largest. Here, 1 m SLR translates in a high water level increase of about 1 m (Figure 4a). Effects of SLR decrease with distance from the sea, especially in the cases with wind set-up. For example, at the confluence from the Nieuwe Maas and Oude Maas (i.e., in the most landward side of the modeling domain), a 1 m increase in SLR translates in a high water level increase of only 0.8–0.9 m under stormy conditions. The differences between locations along the system become very apparent under high discharge conditions, while differences between scenarios with and without wind set-up become minimal under high discharge conditions.

Low water levels increase by more than 1 m in most parts of the delta (Figure 4b). Only in the most landward reach, low water levels increase consequently by less than 1 m. In the seaward part, it is the wind set-up that

21699291, 2023, 4, Downloaded from https://agupubs.onlinelibrary.wiley.com/doi/10.1029/2022JC019578 by Tu Delft, Wiley Online Library on [09/05/2023]. See the Terms and Conditions (https://onlinelibrary.wiley.com/terms-and-conditions) on Wiley Online Library for rules of use; OA articles are governed by the applicable Creative Commons License

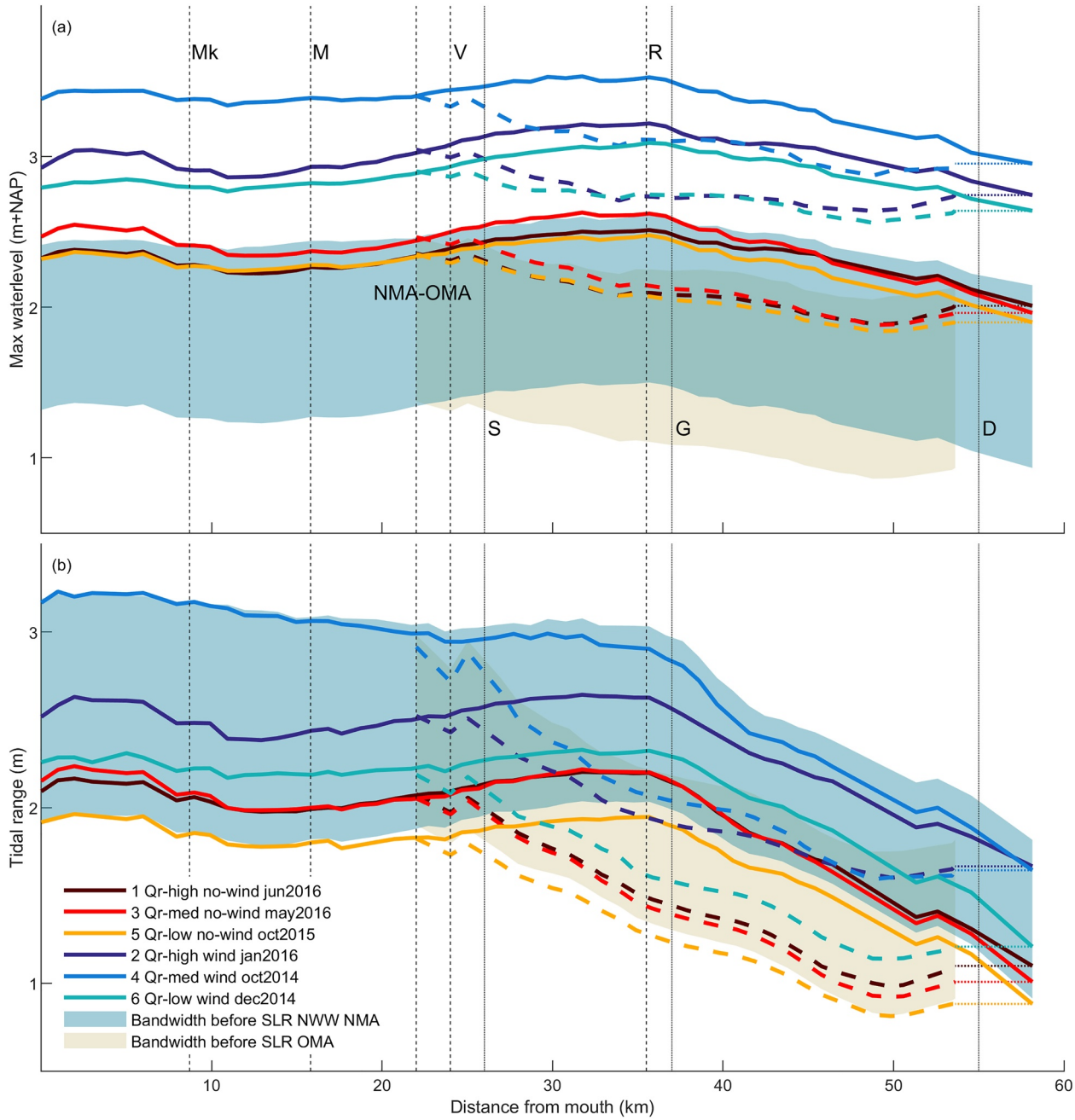

Figure 3. Along-channel variation in (a) maximum water levels and (b) tidal range. Shaded areas indicate the present bandwidth of occurring conditions as obtained from Figure 2. The lines indicate the same scenarios as in Figure 2 with 1 m sea-level rise. Abbreviations are the same as in Figure 2.

determines whether low water levels increase more or less than 1 m. For low and medium discharges, conditions with wind setup result in smaller increases. The largest increases in low water levels are observed in the middle part of the delta, where under low discharge conditions, without wind, the low water levels increase by about 1.05–1.08 m for 1 m SLR. In most places, increasing discharge results in lower low water levels, for cases without wind set-up.

Recent channel deepenings have increased high water levels and future deepenings are expected to do so as well (Figure 5). At the same time, they decrease low water levels, thereby thus significantly amplifying the tide (Figure 5). This was tested by comparing the validation runs (before the most recent deepening of 2019, e.g., V4 in Figure 5) with the reference runs (same conditions, but after the most recent deepening, e.g., R4 in

21699291, 2023, 4, Downloaded from https://agupubs.onlinelibrary.wiley.com/doi/10.1029/2022JC019578 by Tu Delft, Wiley Online Library on [09/05/2023]. See the Terms and Conditions (https://onlinelibrary.wiley.com/terms-and-conditions) on Wiley Online Library for rules of use; OA articles are governed by the applicable Creative Commons License

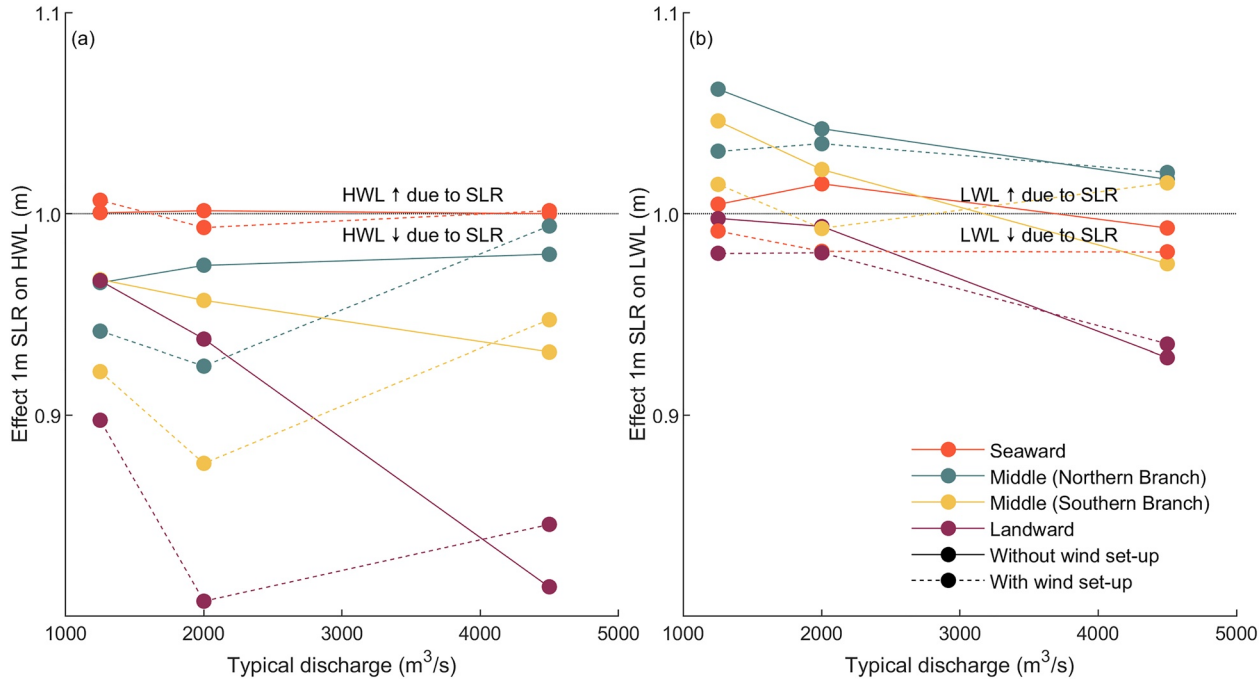

Figure 4. Effect of 1 m sea-level rise on the maximum (left) and minimum (right) water levels along the estuary. Effects depends on the fluvial discharge (*x*-axis), location along the system (indicated by colors) and on the occurrence of wind set-up (indicated by dashed lines).

Figure 5). In addition, this was confirmed by applying a scenario with even further deepening (D4 in Figure 5). Deepening of about 1 m can increase the tidal range with a few centimeters depending on the location along the system. The paradox is that while channel deepening has an amplifying effect on the tides on the short term, deepened channels are less susceptible for future amplification due to SLR. Future shallowing of channels has the potential to reduce high water levels and reduce tidal range (e.g., compare E-SLR with E-SLR-S in Figure 5).

The above illustrates that SLR, wind-induced water level set-up, fluvial discharge and bed level geometry have a compounding effect on peak water levels. Ignoring any of those, may lead to a significant misrepresentation of future coastal flooding hazard (Moftakhari et al., 2017; Ralston et al., 2019).

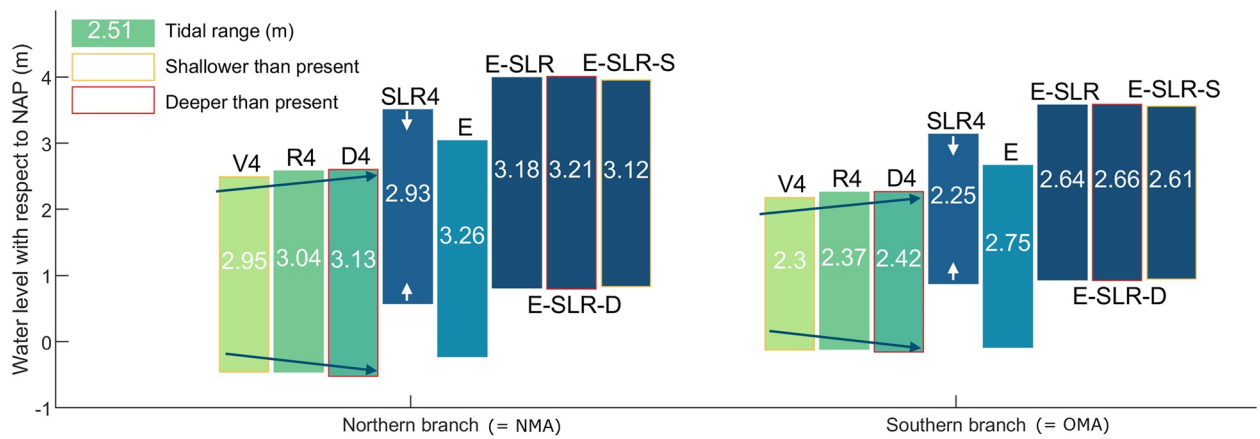

Figure 5. Effect of deepening, shallowing, sea-level rise and extreme conditions on low water levels, high water levels and tidal range. Bars correspond to the tidal range, with the value of the tidal range indicated in white. Yellow outlines indicate model runs in which the channels are shallower than present (≈1 m), red outlines indicate model runs in which the channels are deeper than present (≈1 m). NMA indicates the Nieuwe Maas and OMA the Oude Maas. The color shading of the bars is for visualization purposes only (with darker tones loosely indicating higher high water levels) and has no further detailed meaning.

21699291, 2023, 4, Downloaded from https://agupubs.onlinelibrary.wiley.com/doi/10.1029/2022JC019578 by Tu Delft, Wiley Online Library on [09/05/2023]. See the Terms and Conditions (https://onlinelibrary.wiley.com/terms-and-conditions) on Wiley Online Library for rules of use; OA articles are governed by the applicable Creative Commons License

21699291, 2023, 4, Downloaded from https://agupubs.onlinelibrary.wiley.com/doi/10.1029/2022JC019578 by Tu Delft, Wiley Online Library on [09/05/2023]. See the Terms and Conditions (https://onlinelibrary.wiley.com/terms-and-conditions) on Wiley Online Library for rules of use; OA articles are governed by the applicable Creative Commons License

4.3. Mechanistic Explanation of Deepening and SLR-Effects

Whether or not the tidal range amplifies, remains constant or dampens, depends on width convergence (β), depth convergence (γ) and bed friction (van Rijn, 2011), in which β and γ are inverse length scales for width and depth convergence. Those factors control energy convergence and dissipation per unit width, leading to amplification or dampening of tide. We rewrite the one-dimensional tidal energy balance equation (van Rijn, 2011) to obtain an explicit relation for local along-channel changes in tidal range:

$$\frac{dH}{dx} = -0.5\frac{db/dx}{b}H - 0.5\frac{dh/dx}{h}H - \frac{fu^2}{3\pi gh\cos\phi}, \tag{2}$$

in which b is width, h is depth, x is the channel coordinate, H is tidal range, u is cross-section average flow velocity amplitude, g is gravity acceleration ($g = 9.81$ m/s^2), f is the friction coefficient and ϕ is the phase difference between the horizontal and vertical tide. f is given by $f = 8$ g/C^2, where C is the Chézy coefficient. Equation 2 allows to explain why peak water levels do not increase on par with SLR.

The equation consists of three parts: the tide amplifies when channel width decreases (term I), when channel depth decreases (term II), or when friction decreases (term III). Let us assume the case of local channel deepening for purposes of shipping near the mouth of a delta channel. Then, term I remains approximately constant, term II increases where the depth increases and vice versa, and friction becomes weaker (term III), overall all favoring amplification of the tidal motion. When channel depth uniformly increases due to SLR, dh/dx remains the same while h increases, which reduces tidal amplification (term II). At the same time, friction decreases, reducing tidal dampening (term III). As with channel deepening, width variations (term I) will remain approximately the same in urbanized deltas, where intertidal areas have been reclaimed for land use and channels are fixed by embankment. In deltas with deep channels, the effect of SLR on term II will be much larger than the effect on term III, as an even larger depth will only have a slight reduction of the friction.

All terms in Equation 2 have been calculated for the RMD-system to theoretically assess the effects of SLR and channel deepening on tidal amplification (Supporting Information S1). This calculation is based on the model input, which has been simplified to yield one characteristic value for the main channel featuring side channels, bifurcations and harbors. The simplified calculation qualitatively confirms the theoretical reasoning outlined above. The orders of magnitude of increased tidal amplification due to channel deepening and reduced tidal amplification due to SLR are in line with the model results. The above equation has been implemented in a spreadsheet, which is made available in Supporting Information S1 to estimate the first-order effect of SLR and human interventions on amplification in tidal channels subject to depth convergence by deepening.

5. Discussion and Implications for Sustainable Management of Deltas Worldwide

The results lead us to conclude that peak water levels do not rise on par with SLR in tidal channels subject to depth convergence by deepening. This means that flood risk increases less than what may be expected from the increase in mean sea-level. Only in the most seaward zone, the rise in high water levels approximately matches the rise in mean sea level (Figure 4). Nevertheless, with 1 m of SLR, peak water levels will extend far beyond the present day natural variation (approximate range of 1.5–2.5 m now, vs. 2.5–3.5 after SLR, Figure 3).

Paradoxically, channel deepening has an amplifying effect on the tides on the short term, but deepened channels are less susceptible for future amplification due to SLR. Halting deepening or bringing maintenance dredging to an end, would allow river deltas to become more shallow again, which has been found to be a mitigation strategy and adaptation pathway for estuaries (Familkhalili & Talke, 2016; Orton et al., 2015). These studies found that shallowing (or deepening) of a lagoon type estuary can greatly reduce (raise) extreme water levels for locations susceptible to tropical cyclones. However, our results imply that those measures have only a limited effect on decreasing future flood risk for already deep convergent channels, for example, by reducing peak water levels with only a few centimeters.

It is worth to explore whether other mitigation strategies, such as creating more space and intertidal area surrounding urbanized river deltas (Cox et al., 2022; Khojasteh et al., 2021; Schuerch et al., 2018; Temmerman & Kirwan, 2015) will have a larger contribution to dampening of the tide. Considering that sea levels will rise substantially in the coming decades, indeed a much wider range of mitigation strategies and adaptation pathways

21699291, 2023, 4, Downloaded from https://agupubs.onlinelibrary.wiley.com/doi/10.1029/2022JC019578 by Tu Delft, Wiley Online Library on [09/05/2023]. See the Terms and Conditions (https://onlinelibrary.wiley.com/terms-and-conditions) on Wiley Online Library for rules of use; OA articles are governed by the applicable Creative Commons License

can be considered to address the prospective SLR impacts on urbanizing deltas such the one considered herein (Haasnoot et al., 2013; Kwadijk et al., 2010).

For engineered deltas with large channel depth, the effects of SLR on peak water levels will be smaller than the anticipated 1 m of SLR (e.g., 0.8–0.9 m increase for the considered case). A similar effect was found for the Blyth estuary (Suffolk, eastern England) (French, 2008), and a simplified analysis of 36 estuaries worldwide confirms that this effect predominantly holds for relatively deep estuaries and deltaic channels (Leuven et al., 2019). This implies that the fate of shallow deltaic channels is probably very different, because they have not yet experienced the same degree of urbanization and deepening as for example, the RMD, the Pearl Delta (Bao et al., 2022) and the Yangtze Delta (Chen et al., 2016; Zhang et al., 2019).

In contrast to deltas with deep channels, shallow channels in more pristine deltas are typically friction-dominated. There, SLR has a larger impact on Term III in Equation 2 than in engineered deltas. For those deltas, a 1 m increase in water depth results in a relatively large reduction in friction (Friedrichs & Aubrey, 1988), which causes tidal amplification. Indeed, simplified models have shown that maximum water levels in those systems increase by 0.3–0.8 m on top of the increase in mean sea level (Leuven et al., 2019), which is predominantly due to reduction of friction. Therefore, peak water levels may rise more than mean sea level if a delta is deepened or dredged for the first time, converting it from a shallow friction-dominated system to one where convergence causes strong amplification.

Lastly, an important result from this study is the decreasing tidal range as a result of SLR. When the tidal range decreases, the tidal prism also reduces, which is the volume of water flowing in and out of the delta over a tidal cycle. Classical stability relations show a relation between cross-sectional area of channels and the tidal prism (Eysink, 1990; Gisen & Savenije, 2015; Jarrett, 1976). While this balance is largely disturbed in deepened deltas by channels being too large (Cox, Huismans, et al., 2021), the stability relations imply that natural shallowing will occur in those systems, if sufficient sediment is available. Moreover, a reduced tidal prism also reduces mixing and increases stratification, all enhancing sedimentation (Chernetsky et al., 2010; Winterwerp, 2011). Currently, channel depth is maintained by dredging for navigation, but adaptation pathways that require shallowing or sedimentation may benefit from the decreased tidal prisms.

6. Conclusions

Analysis of sea-level-rise (SLR) scenarios in the RMD reveals that flood risk increases less than the projected increase in mean sea-level. The expected tidal amplification caused by the increasing water depth is compensated by the decreasing channel depth convergence after SLR. Our mechanistic explanation shows that this effect is relevant for deep channels, which are typically engineered shipping channels as present in urbanized deltas worldwide. This interpretation offers first-order understanding, which can be combined with more conceptual and simplified studies to arrive at conclusions for systems other than the RMD. Contrary to the effect of SLR, local channel deepening has an amplifying effect on the tides on the short term, but deepened channels are less vulnerable to tidal amplification due to future SLR. Nevertheless, the effect of 1 m SLR extends far beyond the range of present day seasonal variations and the amount of tidal damping caused by mitigating measures. This implies only a minor part of the SLR-effects can be mitigated if channels are allowed to shallow in the coming decades. Considering that in the long run—even with the average of the bandwidth in RCP2.6—the sea level is expected to rise with more than 1 m, the results in this study imply that SLR effects will at some point overwhelm human interference. As many estuaries and deltas globally are undergoing similar changes as the RMD (engineering works, dredging for port access, embankments and dikes for flood protection), it represents a new state for estuaries. Hence, our work can provide new insights for this and similar systems which cannot be captured by classic estuary research.

Conflict of Interest

The authors declare no conflicts of interest relevant to this study.

Data Availability Statement

All data are open access available in the figures, tables, and supplement and the corresponding data will be uploaded in a repository once the article is accepted. We validated the model results with data from measurement stations within the modeling domain (Figure 1b). Measured water levels at those stations and wind conditions

at the seaward boundary (Hoek van Holland) were available from Rijkswaterstaat (waterinfo.rws.nl and noos.matroos.rws.nl). Validation results are shown in the supplementary material. Numerical models including bed level files, data used for validation, and scripts to process the data and create the figures are available through Zenodo (https://doi.org/10.5281/zenodo.7736026).

Acknowledgments
This research was supported by the Dutch Technology Foundation TTW (grant Vici 17062 to AJFH), which is part of the Netherlands Organisation for Scientific Research (NWO), and is partly funded by the Ministry of Economic Affairs. This work was part of the PhD research project of IN, which is part of the Rivers2Morrow research program and as such is funded by the Ministry of Infrastructure and Water Management.

References

Ashworth, P. J., Best, J. L., & Parsons, D. R. (2015). *Fluvial-tidal sedimentology* (Vol. 68). Elsevier.
Bao, S., Zhang, W., Qin, J., Zheng, J., Lv, H., Feng, X., et al. (2022). Peak water level response to channel deepening depends on interaction between tides and the river flow. *Journal of Geophysical Research: Oceans*, *127*(4), e2021JC017625. https://doi.org/10.1029/2021jc017625
Bendixen, M., Best, J., Hackney, C., & Iversen, L. L. (2019). *Time is running out for sand*. Nature Publishing Group.
Buchanan, M. K., Oppenheimer, M., & Kopp, R. E. (2017). Amplification of flood frequencies with local sea level rise and emerging flood regimes. *Environmental Research Letters*, *12*(6), 064009. https://doi.org/10.1088/1748-9326/aa6cb3
Cai, H., Savenije, H. H., & Toffolon, M. (2012). A new analytical framework for assessing the effect of sea-level rise and dredging on tidal damping in estuaries. *Journal of Geophysical Research*, *117*(C9). https://doi.org/10.1029/2012jc008000
Chen, W., Chen, K., Kuang, C., Zhu, D. Z., He, L., Mao, X., et al. (2016). Influence of sea level rise on saline water intrusion in the Yangtze River Estuary, China. *Applied Ocean Research*, *54*, 12–25. https://doi.org/10.1016/j.apor.2015.11.002
Chernetsky, A. S., Schuttelaars, H. M., & Talke, S. A. (2010). The effect of tidal asymmetry and temporal settling lag on sediment trapping in tidal estuaries. *Ocean Dynamics*, *60*(5), 1219–1241. https://doi.org/10.1007/s10236-010-0329-8
Cox, J. R., Dunn, F., Nienhuis, J., van der Perk, M., & Kleinhans, M. (2021). Climate change and human influences on sediment fluxes and the sediment budget of an urban delta: The example of the lower Rhine-Meuse Delta distributary network. *Anthropocene Coasts*, *4*(1), 251–280. https://doi.org/10.1139/anc-2021-0003
Cox, J. R., Huismans, Y., Knaake, S., Leuven, J. R. F. W., Vellinga, N. E., van der Vegt, M., et al. (2021b). Anthropogenic effects on the contemporary sediment budget of the lower Rhine-Meuse Delta channel network. *Earth's Future*, *9*(7). https://doi.org/10.1029/2020ef001869
Cox, J. R., Paauw, M., Nienhuis, J. H., Dunn, F. E., van der Deijl, E., Esposito, C., et al. (2022). A global synthesis of the effectiveness of sedimentation-enhancing strategies for river deltas and estuaries. *Global and Planetary Change*, *214*, 103796. https://doi.org/10.1016/j.gloplacha.2022.103796
Cox, J. R., Leuven, J. R. F. W., Pierik, H. J., van Egmond, M., & Kleinhans, M. (2022b). Sediment deficit and morphological change of the Rhine-Meuse river mouth attributed to multi-millennial anthropogenic impacts. *Continental Shelf Research*, *244*, 104766. https://doi.org/10.1016/j.csr.2022.104766
Cox, J. R., Lingbeek, J., Weisscher, S. A. H., & Kleinhans, M. G. (2022). Effects of sea-level rise on dredging and dredged estuary morphology. *Journal of Geophysical Research: Earth Surface*, *127*(10), e2022JF006790. https://doi.org/10.1029/2022jf006790
De Goede, E. D. (2020). Historical overview of 2D and 3D hydrodynamic modelling of shallow water flows in The Netherlands. *Ocean Dynamics*, *70*(4), 521–539. https://doi.org/10.1007/s10236-019-01336-5
Deltares. (2014). Delft3D-WAVE user manual. Version 3.05.34160
Deltares. (2021). Delft3D-FLOW user manual. Version 3.15.
de Vriend, H. J., Wang, Z. B., Ysebaert, T., Herman, P. M., & Ding, P. (2011). Eco-morphological problems in the Yangtze Estuary and the Western Scheldt. *Wetlands*, *31*(6), 1033–1042. https://doi.org/10.1007/s13157-011-0239-7
Duits, M., & Kuijper, B. (2017). *Hydra-NL Systeemdocumentatie. Versie 2.3*. (Tech. Rep. No. PR3506). HKV Lijn in Water.
Edmonds, D. A., Caldwell, R. L., Brondizio, E. S., & Siani, S. M. (2020). Coastal flooding will disproportionately impact people on river deltas. *Nature Communications*, *11*(1), 1–8. https://doi.org/10.1038/s41467-020-18531-4
Eysink, W. D. (1990). Morphologic response of tidal basins to changes. *Coastal Engineering Proceedings*, *1*(22), 1948–1961. https://doi.org/10.1061/9780872627765.149
Familkhalili, R., & Talke, S. A. (2016). The effect of channel deepening on tides and storm surge: A case study of Wilmington, NC. *Geophysical Research Letters*, *43*(17), 9138–9147. https://doi.org/10.1002/2016gl069494
Familkhalili, R., Talke, S. A., & Jay, D. A. (2020). Tide-storm surge interactions in highly altered estuaries: How channel deepening increases surge vulnerability. *Journal of Geophysical Research: Oceans*, *125*(4), e2019JC015286. https://doi.org/10.1029/2019jc015286
French, J. (2008). Hydrodynamic modelling of estuarine flood defence realignment as an adaptive management response to sea-level rise. *Journal of Coastal Research*, *24*(10024), 1–12. https://doi.org/10.2112/05-0534.1
Friedrichs, C. T., & Aubrey, D. G. (1988). Non-linear tidal distortion in shallow well-mixed estuaries: A synthesis. Estuarine. *Coastal and Shelf Science*, *27*(5), 521–545. https://doi.org/10.1016/0272-7714(88)90082-0
Friedrichs, C. T., Aubrey, D. G., & Speer, P. E. (1990). Impacts of relative sea-level rise on evolution of shallow estuaries. In *Residual currents and long-term transport* (pp. 105–122). Springer.
Ganguli, P., & Merz, B. (2019). Extreme coastal water levels exacerbate fluvial flood hazards in Northwestern Europe. *Scientific Reports*, *9*(1), 1–14. https://doi.org/10.1038/s41598-019-49822-6
Giosan, L., Syvitski, J., Constantinescu, S., & Day, J. (2014). Comment: Protect the world's deltas. *Nature*, *516*(7529), 31–33. https://doi.org/10.1038/516031a
Gisen, J. I. A., & Savenije, H. H. G. (2015). Estimating bankfull discharge and depth in ungauged estuaries. *Water Resources Research*, *51*(4), 2298–2316. https://doi.org/10.1002/2014WR016227
Haasnoot, M., Bouwer, L., Diermanse, F., Kwadijk, J., Van der Spek, A., Essink, G. O., et al. (2018). *Mogelijke gevolgen van versnelde zeespiegelstijging voor het deltaprogramma: een verkenning*. Deltares Delft.
Haasnoot, M., Kwakkel, J. H., Walker, W. E., & ter Maat, J. (2013). Dynamic adaptive policy pathways: A method for crafting robust decisions for a deeply uncertain world. *Global Environmental Change*, *23*(2), 485–498. https://doi.org/10.1016/j.gloenvcha.2012.12.006
Hackney, C. R., Darby, S. E., Parsons, D. R., Leyland, J., Best, J. L., Aalto, R., et al. (2020). River bank instability from unsustainable sand mining in the lower mekong river. *Nature Sustainability*, *3*(3), 217–225. https://doi.org/10.1038/s41893-019-0455-3
Hoitink, A. J. F., Nittrouer, J. A., Passalacqua, P., Shaw, J. B., Langendoen, E. J., Huismans, Y., & van Maren, D. S. (2020). Resilience of river deltas in the anthropocene. *Journal of Geophysical Research: Earth Surface*, *125*(3). https://doi.org/10.1029/2019jf005201
Huismans, Y., Koopmans, H., Wiersma, A., de Haas, T., Berends, K., Sloff, K., & Stouthamer, E. (2021). Lithological control on scour hole formation in the Rhine-Meuse Estuary. *Geomorphology*, *385*, 107720. https://doi.org/10.1016/j.geomorph.2021.107720

21699291, 2023, 4, Downloaded from https://agupubs.onlinelibrary.wiley.com/doi/10.1029/2022JC019578 by Tu Delft, Wiley Online Library on [09/05/2023]. See the Terms and Conditions (https://onlinelibrary.wiley.com/terms-and-conditions) on Wiley Online Library for rules of use; OA articles are governed by the applicable Creative Commons License

Idier, D., Paris, F., Le Cozannet, G., Boulahya, F., & Dumas, F. (2017). Sea-level rise impacts on the tides of the European shelf. *Continental Shelf Research*, *137*, 56–71. https://doi.org/10.1016/j.csr.2017.01.007

Jarrett, J. T. (1976). *Tidal prism-inlet area relationships*. (Tech. Rep. No. WES-GITI-3). Army Engineer Water Ways Experiment Station.

Khojasteh, D., Glamore, W., Heimhuber, V., & Felder, S. (2021). sea level rise impacts on estuarine dynamics: A review. *Science of The Total Environment*, *780*, 146470. https://doi.org/10.1016/j.scitotenv.2021.146470

Kramer, N., Smale, A., den Bieman, J., & Chbab, H. (2017). *Hydraulische belasting benedenrivieren*. (Tech. Rep. No. 1230087-004-HYE-0001). Deltares.

Kranenburg, W. (2015a). *Evaluatie van het OSR-model voor zoutindringing in de RIjn-Maasmonding (II)*. (Tech. Rep. No. 1220070-000-ZKS-0009). Deltares.

Kranenburg, W. (2015b). *Evaluatie van het OSR-model voor zoutindringing in de Rijn-Maasmonding (I)*. (Tech. Rep. No. 1209459-000-ZKS-0028). Deltares.

Kroos, J. (2014). *Stormvloedrapport van 5 t/m 7 december 2013 (sr91). sint-nicolaasvloed 2013*. (Tech. Rep.). WMCN-KUST.

Kwadijk, J. C. J., Haasnoot, M., Mulder, J. P. M., Hoogvliet, M. M. C., Jeuken, A. B. M., van der Krogt, R. A. A., et al. (2010). Using adaptation tipping points to prepare for climate change and sea level rise: A case study in The Netherlands. *Wiley Interdisciplinary Reviews: Climate Change*, *1*(5), 729–740. https://doi.org/10.1002/wcc.64

Lenderink, G., Buishand, A., & Van Deursen, W. (2007). Estimates of future discharges of the river Rhine using two scenario methodologies: Direct versus delta approach. *Hydrology and Earth System Sciences*, *11*(3), 1145–1159. https://doi.org/10.5194/hess-11-1145-2007

Leuven, J. R. F. W., Pierik, H. J., van der Vegt, M., Bouma, T. J., & Kleinhans, M. G. (2019). Sea-level-rise-induced threats depend on the size of tide-influenced estuaries worldwide. *Nature Climate Change*, *9*(12), 986–992. https://doi.org/10.1038/s41558-019-0608-4

Leuven, J. R. F. W., van Maanen, B., Lexmond, B. R., van der Hoek, B. V., Spruijt, M. J., & Kleinhans, M. G. (2018). Dimensions of fluvial-tidal meanders: Are they disproportionally large? *Geology*, *46*(10), 923–926. https://doi.org/10.1130/G45144.1

Masson-Delmotte, V., Zhai, P., Pirani, A., Connors, S., Péan, C., Berger, S., et al. (2021). *IPCC, 2021: Climate change 2021: The physical science basis. Contribution of working group I to the sixth assessment report of the intergovernmental panel on climate change*. Report. IPCC.

Minderhoud, P., Coumou, L., Erban, L., Middelkoop, H., Stouthamer, E., & Addink, E. (2018). The relation between land use and subsidence in the Vietnamese Mekong delta. *Science of The Total Environment*, *634*, 715–726. https://doi.org/10.1016/j.scitotenv.2018.03.372

Moftakhari, H. R., Salvadori, G., AghaKouchak, A., Sanders, B. F., & Matthew, R. A. (2017). Compounding effects of sea level rise and fluvial flooding. *Proceedings of the National Academy of Sciences*, *114*(37), 9785–9790. https://doi.org/10.1073/pnas.1620325114

Muñoz, D. F., Moftakhari, H., Kumar, M., & Moradkhani, H. (2022). Compound effects of flood drivers, sea level rise, and dredging protocols on vessel navigability and wetland inundation dynamics. *Frontiers in Marine Science*, *9*. https://doi.org/10.3389/fmars.2022.906376

O'Neill, A. C., Erikson, L. H., & Barnard, P. L. (2020). Impacts of sea-level rise on the tidal reach of California coastal rivers using the coastal storm modeling system (CoSMoS). *Journal of Coastal Research*, *95*(SI), 1223–1228. https://doi.org/10.2112/si95-237.1

Oppenheimer, M., & Hinkel, J. (2019). Sea level rise and implications for low lying islands, coasts and communities supplementary material. IPCC special report on the ocean and cryosphere in a changing climate.

Orton, P. M., Conticello, F., Cioffi, F., Hall, T., Georgas, N., Lall, U., et al. (2020). Flood hazard assessment from storm tides, rain and sea level rise for a tidal river estuary. *Natural Hazards*, *102*(2), 729–757. https://doi.org/10.1007/s11069-018-3251-x

Orton, P. M., Talke, S. A., Jay, D. A., Yin, L., Blumberg, A. F., Georgas, N., et al. (2015). Channel shallowing as mitigation of coastal flooding. *Journal of Marine Science and Engineering*, *3*(3), 654–673. https://doi.org/10.3390/jmse3030654

Pickering, M., Horsburgh, K., Blundell, J., Hirschi, J.-M., Nicholls, R. J., Verlaan, M., & Wells, N. (2017). The impact of future sea-level rise on the global tides. *Continental Shelf Research*, *142*, 50–68. https://doi.org/10.1016/j.csr.2017.02.004

Portner, H. O., Roberts, D. C., Adams, H., Adler, C., Aldunce, P., Ali, E., et al. (2022). Climate change 2022: Impacts, adaptation and vulnerability.

Purvis, M. J., Bates, P. D., & Hayes, C. M. (2008). A probabilistic methodology to estimate future coastal flood risk due to sea level rise. *Coastal Engineering*, *55*(12), 1062–1073. https://doi.org/10.1016/j.coastaleng.2008.04.008

Quante, M., & Colijn, F. (2016). *North sea region climate change assessment*. Springer Nature.

Ralston, D. K., Talke, S., Geyer, W. R., Al-Zubaidi, H. A., & Sommerfield, C. K. (2019). Bigger tides, less flooding: Effects of dredging on barotropic dynamics in a highly modified estuary. *Journal of Geophysical Research: Oceans*, *124*(1), 196–211. https://doi.org/10.1029/2018jc014313

Schuerch, M., Spencer, T., Temmerman, S., Kirwan, M. L., Wolff, C., Lincke, D., et al. (2018). Future response of global coastal wetlands to sea-level rise. *Nature*, *561*(7722), 231–234. https://doi.org/10.1038/s41586-018-0476-5

Syvitski, J. P., Kettner, A. J., Overeem, I., Hutton, E. W., Hannon, M. T., Brakenridge, G. R., et al. (2009). Sinking deltas due to human activities. *Nature Geoscience*, *2*(10), 681–686. https://doi.org/10.1038/ngeo629

Talke, S. A., Familkhalili, R., & Jay, D. A. (2021). The influence of channel deepening on tides, river discharge effects, and storm surge. *Journal of Geophysical Research: Oceans*, *126*(5), e2020JC016328. https://doi.org/10.1029/2020jc016328

Talke, S. A., & Jay, D. A. (2020). Changing tides: The role of natural and anthropogenic factors. *Annual Review of Marine Science*, *12*(1), 121–151. https://doi.org/10.1146/annurev-marine-010419-010727

Temmerman, S., & Kirwan, M. L. (2015). Building land with a rising sea. *Science*, *349*(6248), 588–589. https://doi.org/10.1126/science.aac8312

Temmerman, S., Meire, P., Bouma, T. J., Herman, P. M., Ysebaert, T., & De Vriend, H. J. (2013). Ecosystem-based coastal defence in the face of global change. *Nature*, *504*(7478), 79–83. https://doi.org/10.1038/nature12859

van Dijk, W. M., Cox, J., Leuven, J. R. F. W., Cleveringa, J., Taal, M., Hiatt, M. R., et al. (2021). The vulnerability of tidal flats and multi-channel estuaries to dredging and disposal. *Anthropocene Coasts*, *4*(1), 36–60. https://doi.org/10.1139/anc-2020-0006

van Dorland, R. (2021). *Knmi klimaatsignaal 2021: Hoe het klimaat in nederland snel verandert*. (Tech. Rep.). KNMI.

van Rijn, L. C. (2011). Analytical and numerical analysis of tides and salinities in estuaries; Part I: Tidal wave propagation in convergent estuaries. *Ocean Dynamics*, *61*(11), 1719–1741. https://doi.org/10.1007/s10236-011-0453-0

Vellinga, N. E., Hoitink, A. J. F., van der Vegt, M., Zhang, W., & Hoekstra, P. (2014). Human impacts on tides overwhelm the effect of sea level rise on extreme water levels in the Rhine–Meuse delta. *Coastal Engineering*, *90*, 40–50. https://doi.org/10.1016/j.coastaleng.2014.04.005

Winterwerp, J. C. (2011). Fine sediment transport by tidal asymmetry in the high-concentrated ems river: Indications for a regime shift in response to channel deepening. *Ocean Dynamics*, *61*(2), 203–215. https://doi.org/10.1007/s10236-010-0332-0

Wu, Z., Saito, Y., Zhao, D., Zhou, J., Cao, Z., Li, S., et al. (2016). Impact of human activities on subaqueous topographic change in Lingding Bay of the Pearl River estuary, China, during 1955–2013. *Scientific Reports*, *6*(1), 1–10. https://doi.org/10.1038/srep37742

21699291, 2023, 4, Downloaded from https://agupubs.onlinelibrary.wiley.com/doi/10.1029/2022JC019578 by Tu Delft, Wiley Online Library on [09/05/2023]. See the Terms and Conditions (https://onlinelibrary.wiley.com/terms-and-conditions) on Wiley Online Library for rules of use; OA articles are governed by the applicable Creative Commons License

Yang, Z., Wang, T., Voisin, N., & Copping, A. (2015). Estuarine response to river flow and sea-level rise under future climate change and human development. *Estuarine, Coastal and Shelf Science*, *156*, 19–30. https://doi.org/10.1016/j.ecss.2014.08.015

Zhang, W., Feng, H., Zhu, Y., Zheng, J., & Hoitink, A. J. F. (2019). Subtidal flow reversal associated with sediment accretion in a delta channel. *Water Resources Research*, *55*(12), 10781–10795. https://doi.org/10.1029/2019wr025945

Erratum

In the originally published version of this article, Table 1, part b contained the following errors: "1/10" under the header "Qr" should be "Med (≈2,000)," and "1/10" under the header "Wind" should be "1/100." The errors have been corrected, and this may be considered the authoritative version of record.

21699291, 2023, 4, Downloaded from https://agupubs.onlinelibrary.wiley.com/doi/10.1029/2022JC019578 by Tu Delft, Wiley Online Library on [09/05/2023]. See the Terms and Conditions (https://onlinelibrary.wiley.com/terms-and-conditions) on Wiley Online Library for rules of use; OA articles are governed by the applicable Creative Commons License